RM-309

CORRELATION OF MECHANICAL AND THERMAL PROPERTIES OF EXTRATERRESTRIAL MATERIALS

February 1966

Grumman

RESEARCH DEPARTMENT

GRUMMAN AIRCRAFT ENGINEERING CORPORATION
BETHPAGE NEW YORK

Grumman Research Department Memorandum RM-309

CORRELATION OF MECHANICAL AND THERMAL PROPERTIES OF EXTRATERRESTRIAL MATERIALS

by

J. D. Halajian
J. Reichman

Geo-Astrophysics Section

Second Quarterly Progress Report on Contract NAS 8-20084

February 1966

Approved by: Charles E. Mack, Jr.
Charles E. Mack, Jr.
Director of Research

SUMMARY

This report partially fulfills the reporting requirements of Contract No. NAS 8-20084, and represents the second quarterly progress report on the "Correlation of Mechanical and Thermal Properties of Extraterrestrial Materials." It covers work performed from 28 September 1965 to 28 December 1965.

In the Phase I section, two-layer models of the lunar surface are analyzed in terms of the thermal inertia constant and thickness of the layers. It is found that midnight temperatures sufficiently define these parameters and that for midnight temperatures above 110°K, the two-layer models converge to a homogeneous model for upper layer thicknesses sufficiently large. The importance and urgency of additional analyses and measurements of lunar nighttime temperatures are stressed in view of recent lunar data that suggest the existence of localized areas on the moon that, according to our preliminary estimates, could be sufficiently "soft" and deep to be avoided during a lunar landing.

In the Phase II subsection, analytical expressions for the solid and radiative components of the thermal conductivity of powders have been developed as a function of porosity, particle size, emissivity, and temperature. These models have not yet been verified with experimental data.

In the Phase IIB subsection, the mechanical properties of powders are discussed with particular emphasis on the relatively unexplored "underdense" variety. A mode of failure for such powders is postulated and experimentally verified in an attempt to develop expressions for their bearing strength in terms of material and geometrical parameters that were also used in the analyses of thermal properties. It is hoped that a useful correlation of the thermal and mechanical properties of postulated lunar materials can be made through parameters that are common to both properties.

TABLE OF CONTENTS

LIST OF ILLUSTRATIONS

INTRODUCTION

This second quarterly progress report presents the results of investigations touching upon all phases of the program as originally proposed, including the development of mathematical models for the temperature changes of the lunar surface during a lunation or eclipse and analyses of the thermal and mechanical properties of candidate lunar materials.

In view of present uncertainties in the available lunar thermal data, we are now emphasizing the study of the behavior of various lunar thermal models under given inputs, rather than trying to develop "best fit" models that match a given set of lunar data. The usefulness of this approach is discussed in Phase I and is illustrated with the analysis of two-layer models of the lunar surface in which changes of the thermal inertia constant and thickness of the upper layer are studied as a function of midnight temperatures. The latter parameter emerges as an important and sensitive index of the thermophysical properties of the lunar surface.

Lunar thermal models are not sufficient to define the physical nature of the lunar surface other than suggesting that the outermost layer of the moon, down to a depth of about a decimeter, is porous or in an "underdense" state of packing. Knowledge of the laws of heat flow and of mechanical behavior of porous media under vacuum conditions is necessary to establish, at best, the various combinations of porosity, grain or pore size, and interparticle bond that are consistent with the lunar thermal model. Furthermore, the correlation of thermal and mechanical properties of porous media in vacuo is complicated by the fact that of the conductive and radiative modes of heat transfer, only the former has some bearing on the manner in which the particles touch one another, hence on the mechanical strength of the particle system. Consequently, Phase II of this report is devoted to those aspects of thermal and mechanical behavior of particulate media that are poorly understood, namely, the relative contribution of the conductive and radiative components of heat transfer and the mode of failure of highly porous "fluffy" powders. It is hoped that the equally porous but more conductive "vesicular" model (i.e., where the solid phase is continuous) will be treated in the next progress report.

PROJECT STATUS

Phase I

The first quarterly progress report discussed the background to the measurements of lunar surface temperatures and presented a detailed discussion of the mathematical model used in the computer program. During that reporting period, the program was not completed. During the quarter reported herein, the program has been debugged and can now be used to analyze and interpret infrared thermal emission data. Studies are under way to determine eclipse and lunation temperature variations for various models and combinations of parameters. In this report, we discuss the importance of lunar nighttime temperatures and analyze two-layer models in terms of midnight temperatures. The results of the analysis are evaluated in terms of their "engineering" implications.

Phase IIA

In the first progress report we stressed the importance of knowing the conductive and radiative components of thermal conductivity and outlined an approach to studying these components for the "particulate" and "vesicular" models. Various expressions for both components have been derived for the particulate model only and are presented in this report.

Phase IIB

Problem areas in the study of the mechanical properties of the particulate and vesicular models were discussed in the first progress report. No clear solution to the strength problem of the highly porous version of the particulate model was indicated. Herein, we discuss a hopeful approach to such a solution. An experimental model has been built and tested to gain some insight into the failure of "fluffy" soils. This model has enabled us to identify two components of bearing strength in such soils and their parameters. Remaining areas of investigations are discussed at the end of each phase.

PHASE I: THERMOPHYSICAL ANALYSIS OF LUNAR SURFACE

Purpose

The immediate objective of this phase is not necessarily to determine a thermal inertia constant, γ, that best "fits" the known temperature changes of the lunar surface measured during a lunation or eclipse. Such an attempt would not be very meaningful at this time in view of the inadequacy of and uncertainties in the available lunar data. It is meaningful, however, to study the range and the manner in which a number of relevant material and geometrical factors that have been largely neglected or overlooked in past analyses, affect the behavior of γ. This knowledge could be very useful, we believe, in determining what kind of new lunar data are urgently needed, how the new observations should be made in terms of wavelength, resolution, lunar phase and location on the moon, and what additional information could be derived from the new data in the light of refined theoretical models.

We discuss herein the importance of lunar nighttime temperatures and present the results of analyses on the behavior of γ as a function of midnight temperature and the thickness of the upper layer in a two-layer model.

Importance of Lunar Nighttime Temperature Data

The nighttime temperature is a sensitive index to the thermal inertia parameter γ. During insolation the surface temperature is in near equilibrium with the input solar flux. Large variations in γ will not significantly affect the surface temperature. During the lunar nighttime however, the surface temperature is determined almost exclusively by the thermal parameters of the lunar material. During the penumbral and umbral phases of an eclipse the temperature cooling curves will sensitively depend on the thermal parameters. However, there are other parameters that will also affect the cooling behavior such as roughness, infrared transparency and heat sources as discussed below.

Bastin (Ref. 1) suggests that lunar roughness on a centimeter scale could account for anomalously high temperatures (hot spots) that were uncovered by Saari and Shorthill (Ref. 2) during eclipse cooling. Using a simple roughness model, he calculates an increase of $40^{\circ}K$ in surface temperature as compared to that of a smooth

surface under identical cooling conditions. During the lunar nighttime, the considerably greater cooling times available would require a roughness scale of the order of decimeters to account for hot spots. Radar data indicate a smooth surface at this scale. Roughness can probably be ruled out as a factor in explaining hot spots during the lunar night unless radar data for a hot spot region show anomalously high return. Another possible explanation, offered by Buettner (Ref. 3), to account for eclipse hot spots is that of infrared transparency. During eclipse cooling, there is a large temperature gradient occurring within the first centimeter of the lunar material. Partial transparency of infrared radiation of the material in 8-14 micron range would give misleadingly high surface temperature readings as inferred by radiation sensors. During the lunar night however, the effect of transparency is not nearly as significant. This is due to two reasons: 1) the temperature gradient is considerably more shallow; and 2) the major portion of emission occurs at wavelengths longer than the 8-14 micron atmospheric window.

Regarding a third possibility — whether the observed "hot spots" are due to internal heat sources — it is not clear at this point whether temperature measurements during a lunation could confirm or rule out this hypothesis, which is certainly interesting and deserves more attention.

The apparently less ambiguous use of nighttime temperature in determining γ, coupled with the better detectors available to measure low temperatures at high resolution, present a cogent argument for increasing the meager data presently available. We hope that our analysis will lend further justification for initiating new lunar measurements

Available Lunar Nighttime Temperature Data

Pettit and Nicholson (Ref. 4) made the first determination of nighttime temperatures and obtained a value of 120 ±5°K for the midnight temperature using a vacuum thermocouple. Using more recent atmospheric transmission data, a correction of the midnight temperature to 108°K was made (Ref. 2). Sinton (Ref. 5) determined a midnight temperature of 122 ±3°K for two areas near the limb. Murray and Wildey (Ref. 6) and Saari and Shorthill (Ref. 2) measured nighttime temperatures from which extrapolated midnight temperatures of 106°K and 99°K were obtained. These temperatures can perhaps best be described as upper limits to the midnight temperature. Low (Ref. 7), using a very sensitive bolometer, was able to obtain measurements of midnight temperatures ranging from less than 70°K to over 150°K.

Results of Two-Layer Model Study

The two-layer model was first used by Piddington and Minnett (Ref. 8) to explain their microwave temperature measurements. Since then, this model has been used by several investigators (Jaeger, Ref. 9; Sinton, Ref. 5) to successfully match lunar eclipse cooling curves. Because of the short cooling time during an eclipse, temperature changes occur within the upper centimeter of surface material. Hence, the interpretation of eclipse data in terms of a two-layer model would converge to the homogeneous model for upper layer thicknesses exceeding a few millimeters.

The object of this study is not necessarily to "match" actual lunar data, which at best is meager at this time, but to determine the effect of varying upper layer thicknesses on lunation temperatures as a function of the thermal parameters of both layers. The usefulness of this study, which to our knowledge has not been previously made, resides in the fact that the lunar midnight temperature, by virtue of its greater penetration depth, is a sensitive index of the material properties of the uppermost layer of the moon to as much as 15 centimeters. In addition, this index enables one to eliminate various other explanations that have been offered to account for the recently observed thermal anomalies, as we discussed above.

The two-layer model consists of an upper layer of "soft" insulating material supported by an underlayer of "harder" more conductive material. The following combinations of γ values $\left(\gamma = (k\rho C)^{-\frac{1}{2}}\right)$ were studied (a higher γ value corresponds to a more highly insulating or "softer" material):

Upper Layer γ_0	Lower Layer γ_1
1250	250
1250	20
1000	250
1000	20
750	250
750	20

Figure 1 is a typical plot of lunation temperature as obtained from the IBM-7094 CALCOMP plotter. Temperature is plotted versus lunation time. A lunation time of 0 or 1.0 corresponds to high noon of the lunar day and a lunation time of 0.5 corresponds to midnight. All the curves are for upper and lower layer γ values of 1000 and 250 respectively. The lunar night is in the region between 0.25 and 0.75. As seen from the figure, there is very little difference in the temperature curves during solar insolation for different upper layer thicknesses. During the lunar nighttime ($0.25 \leq t \leq 0.75$) however, the lunation curves show appreciable differences. The thinner the upper layer, the hotter the surface temperature tends to be. This can be explained in the following manner: the thicker the insulating layer, the more effective it is as a barrier to heat flow. The surface temperature reaches a balance controlled by the heat flow radiating from it and the heat flow coming from the interior. As the insulating layer becomes thicker, it effectively prevents more heat from flowing from the interior to the surface, consequently the surface cools more rapidly. An exception to this occurs at the beginning of lunar night. There is a crossing over between the two lowermost curves. Initially the temperature of the thicker layer is higher but then decreases below the temperature of the thinner layer at a lunation time of 0.325. The crossover is caused by the fact that the thermal energy content of the thicker layer is higher at the inception of nighttime. As the influence of this initial condition diminishes with time, the presence of the lower layer becomes dominant resulting in a lower rate of cooling for the surface with a thinner insulating layer.

In Fig. 1, we can readily see that there is very little variation between the various curves of the two-layer models other than in the nighttime region. We may, therefore, use the midnight temperature as a convenient parameter that characterizes a lunation curve. Figures 2 and 3 are plots of midnight temperature versus upper layer thickness. Figure 2 is for a lower layer γ value of 250 with each curve representing a different upper layer γ value. The curves converge to a midnight temperature of 138°K, which represents the results for a homogeneous model with the lower layer γ value of 250. The curves become asymptotic at midnight temperatures ranging from about 90 to 102°K and corresponding to upper layer γ's ranging from 1250 to 750. This asymptotic behavior is due to the attenuation of the thermal heat wave as it progresses through the material. This effectively makes the surface temperature independent of the nature of material below a certain depth. The two-layer model, therefore, converges to the homogeneous model when the upper layer becomes sufficiently thick.

The limitations of midnight temperatures in determining a unique two-layer model is readily apparent. For a given midnight temperature, there is a range of γ values and upper layer thicknesses that are possible. This is illustrated in Fig. 4 where the γ of the upper layer is plotted against the thickness of this layer for a midnight temperature of 110°K. Each curve represents a different lower layer γ value. The curves are asymptotic to a γ value of 580 corresponding to the homogeneous model.

Although the curves in Figs. 1 through 4 speak for themselves, it is interesting to point out that the inability of the midnight temperature to discriminate between the effects of the γ_0 and ℓ_0 parameters of the two-layer model is not a serious limitation because, as the results point out, these two parameters (related to the hardness and depth of the uppermost layer) vary in a "compensating" manner as far as the suitability of the layer is concerned for engineering operations on the moon. We notice in Fig. 4, that for a given midnight temperature, high γ values, representing "soft" materials, are associated with <u>shallow</u> layers of the orders of a few centimeters, overlying a much harder material. Conversely, thermally homogeneous layers, that could range in depth from a few cm to infinity, have to be associated with relatively <u>hard</u> materials ($\gamma_0 = 500$) to satisfy a midnight temperature of 110°K.

It is conceivable, however, that a layer on the lunar surface could be both deep and soft if its midnight temperature is appreciably lower than 110°K. We plan to extend our analysis of the two-layer model to midnight temperatures ranging from 70 to 150°K as recently observed by Low (Ref. 7). These temperatures correspond roughly to materials ranging in hardness from the consistency of "fluff" to that of porous rock. The thermal and mechanical properties of these candidate lunar materials will be analyzed and correlated in Phase II.

The possibility, as revealed by our analysis, that soft and deep layers of the lunar surface could correspond to a midnight temperature of 70°K, plus the probability, as revealed by Low's recent lunar measurements, that such areas could exist on the moon, lend a great deal of scientific importance and engineering urgency for performing additional analyses and high-resolution lunar measurements of the nighttime temperatures of specific areas of the lunar surface.

Future Work

Some of the specific areas in the thermophysical analysis of the lunar surface that need immediate attention are as follows:

- Extend studies of the effect of lunar midnight temperatures on γ and upper layer thickness to cover temperature ranges from 70° to 150°K.

- Introduce temperature dependence in the analysis of the lunar thermal model and evaluate its effect on γ for given midnight temperatures.

- Introduce lateral inhomogeneities in the lunar thermal model (i.e., islands of "hot spots" surrounded by less conductive media) and determine effective γ of model (as functions of the percent distribution and individual γ's of the components) in an attempt to assess the importance of high resolution in earth-based lunar temperature measurements.

We will try to accomplish as much of this work as possible during the remaining period of this contract.

PHASE II: THERMOPHYSICAL ANALYSIS OF HYPOTHETICAL MODELS

Purpose

The main objective of this phase is to determine the mechanical properties, or more specifically the bearing or crushing strength of "particulate" and "vesicular" models, that have γ values corresponding to those of the moon as estimated in Phase I of this work or as updated when new and better observational data become available. Since both the thermal and mechanical properties of our models have common variables such as porosity, grain or pore size, and state of bonding between the solid components, attempts are made to develop analytical or empirical relationships that express thermal conductivity and mechanical strength in terms of these variables. This progress report includes work done on the particulate model only. The solid and radiative components of thermal conductivity are treated in Phase IIA and the mechanical properties are treated in Phase IIB.

Phase IIA: Thermal Properties

Models for Thermal Conductivity of Powders

In a vacuum there are two mechanisms that contribute to heat transport through powdered materials: solid conduction and radiation. Solid conduction takes place both through the particles and between the particles across the contact areas. The relatively small contact areas between the particles in comparison to the particle size introduce a large thermal resistance considerably reducing the effective thermal conductivity of the material. Because of the significance of contact area, an expression for the effective conductivity should necessarily include the area or a parameter relating to it. Unfortunately, the area of contact between real surfaces is a very sensitive function of its degree of roughness, hardness, and applied pressure. For example, soft rough particles should have larger areas of contact than do smooth hard spheres. Despite the rather complex dependence of specific geometry on contact area, the fact that an averaging process occurs for a system of many particles gives some confidence to the belief that a relatively simple model may be useful in predicting the solid conduction component of the thermal conductivity.

Model for Solid Conduction Component

An idealized model consisting of a cubic array of smooth spheres is considered. Heat transfer is considered unidirectional. The contact area between two spheres is assumed to be of circular cross section. A diagram of spheres in contact is shown in Fig. 5. Assuming conduction to take place in the x direction only, at steady state the one dimensional heat conduction equation can be written as

$$\frac{d}{dx}\left(k_s A(x)\,\frac{dT}{dx}\right) = 0 \ , \tag{1}$$

where $A(x)$, the area normal to the direction of heat flow, is given by

$$A(x) = \pi(R^2 - x^2) \ . \tag{2}$$

Substituting for $A(x)$ in Eq. (1) and performing the differentiation results in the following differential equation:

$$(R^2 - x^2)\,\frac{d^2T}{dx^2} - 2x\,\frac{dT}{dx} = 0 \ .$$

Integrating, we obtain

$$\frac{dT}{dx} = \frac{C_2}{R^2 - x^2} \ . \tag{3}$$

Integrating again

$$T = C_1 + \frac{C_2}{R}\tanh^{-1}\left(\frac{x}{R}\right) \ . \tag{4}$$

To evaluate the constants of integration, we use the boundary conditions

$$T = T_1 \quad \text{at} \quad x = R(1 - \beta)^{\frac{1}{2}}$$

$$T = T_2 \quad \text{at} \quad x = -R(1 - \beta)^{\frac{1}{2}}$$

where β is the ratio of the contact radius to the sphere radius. Substituting the boundary conditions in Eq. (4) obtains for the constants of integration

$$C_1 = \frac{(T_1 + T_2)}{2}$$

$$C_2 = \frac{(T_2 - T_1)R}{2 \tanh^{-1}(1 - \beta^2)^{\frac{1}{2}}} .$$

The heat flux is given by the following equation:

$$q = k_s A \frac{dT}{dx} . \tag{5}$$

Substituting Eqs. (2) and (3) in Eq. (5), we obtain

$$q = \frac{k_s \pi (T_2 - T_1)R}{2 \tanh^{-1} (1 - \beta^2)^{\frac{1}{2}}} . \tag{6}$$

To determine the effective conductivity, we equate the heat conduction through a solid occupying the maximum cross-sectional area of the sphere with the same boundary temperatures to Eq. (6):

$$k_{eff} \frac{4R^2(T_2 - T_1)}{2R(1 - \beta^2)^{\frac{1}{2}}} = \frac{k_s \pi R(T_2 - T_1)}{2 \tanh^{-1}(1 - \beta^2)^{\frac{1}{2}}} .$$

Solving for the effective conductivity,

$$k_{eff} = \frac{k_s \pi (1 - \beta^2)^{\frac{1}{2}}}{4 \tanh^{-1}(1 - \beta^2)^{\frac{1}{2}}} . \tag{7}$$

To evaluate the contact area parameter β, we use the expression derived by Hertz for the radius of contact between two elastic spheres,

$$r = \left(\frac{3}{4}\,\frac{P(1 - \nu^2)R}{E}\right)^{\frac{1}{3}} \tag{8}$$

where P is the compression force, and ν and E are Poisson's ratio and Young's modulus. If the compressive force is due to the weight of n spheres above the contact, then

$$P = n\rho\,\frac{4}{3}\,\pi R^3 g\ , \tag{9}$$

where g is the gravitational constant and ρ is the density.

Substituting Eq. (9) into Eq. (8), the contact parameter β is found to be

$$\beta = \frac{r}{R} = \left(\frac{\pi\rho g(1 - \nu^2)}{2E}\right)^{\frac{1}{3}} d^{\frac{1}{3}}\ ,$$

where d is the depth of the column of spheres and is given by $d \approx 2Rn$. The above equation indicates that the contact area, hence thermal conductivity, increases with depth beneath the surface. Another initially surprising result is that the thermal conductivity for a given thickness is independent of particle size. The decrease in conductivity due to the greater number of contact resistances per unit length with decreasing particle size is offset by the increased conductivity due to an increase in the ratio of contact radius to particle diameter. The dependence on the gravitational constant indicates that an identical bed of particles on the moon would exhibit a lower thermal conductivity than on earth.

The above derivation of the effective solid conductivity of a bed of particles is applicable for a cubic array of spheres that has a porosity of 48 percent. For more random packings, the porosity could be appreciably different. A more porous packing should make the effective solid conductivity lower than that given by Eq. (7). This can be viewed as due to two factors, the decreased number of conduction paths per unit area normal to heat flow and the more tortuous conduction paths. To extend the range of validity of Eq. (7) to the more porous case, we assume that the effective conductivity varies linearly with porosity and approaches zero at 100 percent porosity. The equation resulting from this assumption is then

$$k_{eff}(p) = \frac{(1 - p)k_s\pi(1 - \beta^2)^{\frac{1}{2}}}{2\ \tanh^{-1}(1 - \beta^2)^{\frac{1}{2}}},$$

where p is the void fraction.

Another equation that relates conductivity to contact area between particles is the Riemann equation (Ref. 10), viz,

$$k = \frac{k_s}{\frac{R}{r} + \frac{1}{\pi}\ \ell n\ \frac{2R}{r}}.$$

The equation developed in this study and the Riemann equation should be compared with experimental data to determine which is the more valid.

Models for Radiative Conduction Component

As the solid conductivity for powdered materials in a vacuum is quite small, the relative contribution of radiation to heat transport may be quite significant even at the modest temperature ranges (100°K-400°K) of interest to this study.

A general treatment of radiative transport in powders is extremely difficult because of the number and nature of the mechanisms involved. Processes of absorption, emission, scattering, and transmission of electromagnetic radiation are involved. These processes are characterized by parameters that are dependent upon the geometry and material properties of the medium. The dominant mechanisms of radiative transport may be significantly different for powders of differing physical properties. In addition, since radiation occurs over a range of wavelengths and the characterizing parameters are generally wavelength dependent, the dominant mechanisms of transport may significantly change with temperature of the media. The utility of a generalized treatment would very much depend on a detailed knowledge of these parameters.

The highly speculative nature of the lunar surface material makes it unwarranted to consider the case of radiative transport to the degree of sophistication that has appeared in the recent literature (Ref. 11). Instead, two approximate methods will be

considered for evaluating the radiative transport. The first can be considered an idealized discrete model where only radiation between surfaces is considered. Three such models are considered. The second approach is to homogenize the particulate medium and thus allow a formulation of the energy transport processes by differential equations. A discussion of the two methods follows.

Discrete Model for Radiative Transport

Layered Slab Model: A powder medium is a rather complex arrangement of oddly shaped grains and interstices. To obtain a model that can be treated analytically, a rather drastic modification of this picture seems to be required. The first model that will be considered is one suggested by Wesselinck (Ref. 12). The lunar surface material is considered stratified into parallel slabs of uniform thickness as shown in Fig. 6.

In this model, s corresponds to the sum of the average dimensions of grain and interstices. The temperature difference between the faces of a slab of solid material is considered negligible because of the relatively high conductivity. The rate of heat transfer between adjacent slabs is given by

$$q = \frac{\epsilon\sigma}{2 - \epsilon}\left(T_1^4 - T_2^4\right) ,$$

where the factor $\epsilon/(2- \epsilon)$ is obtained by considering multiple reflections between the slabs and using Kirchoff's law. For small distances between slabs, the above equation can be approximated by using a derivative:

$$q \approx \frac{\epsilon\sigma}{2 - \epsilon}\frac{\partial T^4}{\partial x}\, s = \frac{4\epsilon\sigma T^3}{2 - \epsilon}\frac{\partial T}{\partial x}\, s ,$$

where $\partial T/\partial x$ refers to the average gradient.

The radiative conductivity is then

$$k_{rad} = \frac{4\epsilon\sigma s T^3}{2 - \epsilon} .$$

To obtain an expression in terms of particle size and porosity we use the relation

$$1 - p = \frac{D}{s} ,$$

and obtain for the conductivity

$$k_{rad} = \frac{4\sigma\epsilon DT^3}{(2 - \epsilon)(1 - p)} . \tag{10}$$

Cubic Particle Model: Other models for radiative conductivity with assumptions in the spirit of that used above have been employed in other studies. Laubitz (Ref. 13) assumes the particles as cubes randomly scattered in cubical volumes but with the faces of two cubes remaining parallel. Based on this model he derives the following equation:

$$k_{rad} = \frac{4\sigma\epsilon DT^3}{1 - p}\left[1 - (1 - p)^{2/3} + (1 - p)^{4/3}\right] . \tag{11}$$

Spherical Particle Model: Schotte (Ref. 14) obtains an equation for the radiative conductivity by considering radiation between the voids of packed spheres and radiation from the particle in series with conduction through the particle. The radiative conductivity is given by

$$k_{rad} = \frac{1 - p}{\frac{1}{k_s} + \frac{1}{k_r^o}} + pk_r^o , \tag{12}$$

where $k_r^o = 4\sigma\epsilon DT^3$ and k_s is the conductivity of the solid material.

The three expressions for the radiative conductivity have similar characteristics. They all display a linear variation of conductivity with particle size, a cubic dependence on temperature, and an increasing conductivity with increasing porosity. The major difference is the manner in which the conductivity

varies with porosity. Figure 7 illustrates the dependence of radiative conductivity on porosity for the three equations. Equation (12) exhibits a linear variation of conductivity with porosity the slope of the curve depending on the ratio of k_r° to the solid conductivity k_s. Equations (10) and (11) display asymptotic behavior at unit porosity. From physical considerations it is apparent that the radiative conductivity should become infinitely large as the porosity approaches unity and that it approaches zero as the porosity approaches zero. It is therefore concluded that Eqs. (10) and (11) give a more realistic picture of the physical situation at high porosities than Eq. (12). A plot of radiative conductivity versus porosity is shown in Fig. 8 for different particle sizes and temperatures.

Homogeneous Model for Radiative Transfer

In interpreting lunar thermal emission data there are two cases in which a homogeneous model for radiative transport appears appropriate. The first case is for a surface material that is transparent to radiation in the infrared region. It has been experimentally established that certain silicate materials are highly transparent to radiation in the infrared (Ref. 15). The other case is that of a surface layer of suspended particles where the distance between particles is large compared to the particle size (Ref. 16). For the case of opaque particles in contact or in near contact, the geometrical model for radiative transport discussed previously appears more appropriate.

By considering the medium to be homogeneous, a description of the energy transport process can be made by differential equations with prescribed boundary conditions. We use a method described by Hamaker (Ref. 17). It consists of dividing the radiative flux into two parts, one flowing in a positive direction and the other in a negative direction. Inherent in this assumption is the compensation of the radiation scattered sideways by equal contributions from neighboring regions. This assumption is reasonable for cases when the area considered is large compared to the thickness and is therefore applicable to a uniform lunar surface layer. Another serious assumption is that the cross sections for absorption and scattering are wavelength independent. This assumption enables one to deal with total radiation thereby greatly simplifying the equations of radiative transfer. The model used is illustrated in Fig. 9. The radiant flux in the positive direction is I and in the negative x direction is J. The surface at

$x = 0$ is assumed at a temperature T_0 with unit emissivity. The suspended particle layer is characterized by macroscopic absorption and scattering cross sections a and s.

The equation for the flux in the positive direction is

$$\frac{dI}{dx} = -(a + s)I + sJ + aE \tag{13}$$

The first term on the right represents the flux loss per unit length due to scattering and absorption and the second term represents an increase due to the backscattering of the negative direction flux. The third term represents the increase in flux gradient due to thermal emission from a volume element dx where

$$E = \sigma T^4$$

and Kirchoff's law $(a = \epsilon)$ is assumed. Similarly for the flux in the negative direction,

$$\frac{dJ}{dx} = (a + s)J - sI - aE \ . \tag{14}$$

An additional equation is given by the energy balance

$$k_s \frac{\partial^2 T}{\partial x^2} + a(I + J) = 2aE \ ,$$

where k_s is the solid component of thermal conductivity. For the suspended particle model $k = 0$, hence,

$$a(I + J) = 2aE \ .$$

Using the above relation in Eqs. (13) and (14) results in the following equations:

$$\frac{dI}{dx} = -\left(\frac{a}{2} + s\right)I + \left(s + \frac{a}{2}\right)J$$

$$\frac{dJ}{dx} = \left(\frac{a}{2} + s\right)J - \left(\frac{a}{2} + s\right)I \ .$$

A solution to the above set of equations is

$$I = (C_2 - C_1)\alpha x + C_1$$

$$J = (C_2 - C_1)\alpha x + C_2 ,$$

where $\alpha = a/2 + s$ and C_1 and C_2 are arbitrary constants. The boundary conditions are

$$x = 0 \qquad I = \sigma T_0^4$$

$$x = L \qquad J = 0$$

The lower boundary condition is due to the assumed black body emission from the surface layer and the upper boundary condition is for the case where there is no solar insolation. Using these boundary conditions to eliminate the arbitrary constants, a solution for the fluxes is

$$I = \frac{\sigma T_0^4 [1 + \alpha(L - x)]}{1 + \alpha L}$$

$$J = \frac{\sigma T_0^4 \alpha (L - x)}{1 + \alpha L} .$$

The net radiation leaving the lunar surface is given by

$$I(x = L) = \frac{\sigma T_0^4}{1 + \alpha L} .$$

From the above equation it can be seen that the suspended particle layer acts to reduce the emissivity of the emitting surface layer. The effective emissivity is given by

$$\epsilon_{eff} = \frac{1}{1 + \alpha L} . \qquad (15)$$

This surprisingly simple result of a decreased emissivity due to a suspended particle layer can be used to interpret lunar emission data without resorting to the use of an equivalent thermal conductivity. By assuming that the thermal relaxation time of the suspended particle layer is small in comparison to lunation times, we can make the so-called adiabatic approximation. This makes it possible to then use the computer program developed for Phase I to calculate lunation temperatures just by varying the surface emissivity. The emissivity used in the computer program can be related to the absorption and scattering cross section and layer thickness given by Eq. (15).

Future Work

A survey of available experimental data on the thermal conductivity of powdered materials in a vacuum is being made. The data will be used to determine the accuracy of the theoretical expressions in predicting the results. If satisfactory agreement is found for these equations or others in the literature, then estimates will be made of the lunar material porosity. This can be done in the following manner: The total effective conductivity which is the sum of the effective radiative and solid conductivities is a function of porosity, particle size, emissivity, and temperature. The solid conductivity, which depends only on porosity and depth, will predominate for particle sizes of less than about 200 microns.

For this case, the total conductivity will depend only upon depth and porosity. We can then proceed in two ways to estimate the porosity of the material. The first method would be to assume a homogeneous model for the lunar surface and determine a porosity based upon an average depth at which lunar nighttime temperatures are affected by the material properties. Assuming solid rock material properties, the porosity can be determined uniquely for a give γ value. The second method would be to use the depth dependent conductivity function in the computer program developed in Phase I and determine a "best fit" porosity.

For the case of large particle sizes where radiation is important, it is necessary to use the computer program with a temperature dependent model to determine the conductivity parameters. The porosity cannot be uniquely determined but can be found as a function of particle size and emissivity.

Phase IIB: Mechanical Properties

Definition of Models

As in the analysis of the thermal properties, the porous models considered in the analysis of the mechanical or strength properties consist of the "particulate" and the "vesicular" varieties. In the former model, discrete particles are mechanically interlocked or bound with relatively weak molecular forces of attraction. In the latter model, the strength is due to solid bridges between particles or elements surrounding concave cavities.

Two versions of the particulate model are considered, namely, those having very dense and very loose packing. These extremes of packing are distinguished because they exhibit basically different modes of failure and orders of magnitude difference in bearing strength or thermal conductivity. The dense versions of the particulate model are representative of conventional, "engineering" soils commonly encountered in nature. Their properties and behavior have been widely investigated. Terzaghi (Ref. 17) has calculated theoretical expressions for their bearing strength in terms of the angle of internal friction of the soil. More emphasis is placed in this work on the underdense versions of the particulate model because they are of greater interest in lunar studies.

Particulate Model

Some of the problems connected with the analysis of this model were discussed in the first progress report. It was pointed out that presently available solutions apply to densely packed versions of the particulate model because the highly porous versions made up necessarily of very fine particles exhibit an entirely different mode of failure. In seeking an analytical solution to this relatively unexplored problem the following approach is now being pursued:

1) Postulate a mode of failure.
2) Verify and refine, qualitatively, the above postulate by means of an experimental model.
3) Identify the important geometrical and force parameters and describe analytically the strength of the underdense particulate medium in terms of these parameters.

Some of the progress made in the first two steps outlined above is discussed in this report.

Postulation of a Mode of Failure

To postulate a mode of failure for the underdense version of the particulate model, it is necessary to determine the boundaries of the disturbed zone, the behavior of the particles within and outside of this zone and the nature and magnitude of the forces that are developed before and during failure. This can be best done by comparing the deformational behavior of the well-known dense (incompressible) medium with the postulated behavior of the underdense (compressible) medium as depicted in Fig. 10. For convenience, these particulate media will be referred to as the cannon ball and the fluffy models. The following postualtions are made:

- Boundaries of the disturbed zone: In the fluffy model, the disturbed zone is limited very nearly to the area immediately under the pad. A vertical wall is sheared as the pad penetrates into the soil. The depth of the compressed material under the pad is unknown. In the cannon ball model, sinkage can take place only through lateral displacement of a mass of soil away from the pad along a shear plane that is nearly horizontal, curved upward at an angle to the surface determined by the coefficient of friction of the soil.

- Behavior of soil within and outside of disturbed zone: As the pad penetrates into the fluffy soil, a "bulb" of compacted material builds up under the pad and increases in thickness as the pad sinks deeper. The rate of the increase in thickness of the bulb with depth and the density profile of the soil within the disturbed zone are not known. In the cannon ball model there is, theoretically, no differential movement of particles within the disturbed mass of soil other than along the plane of failure. During failure, when the particles slide over one another, a slight expansion of volume (called dilatancy) occurs.

- Failure criterion: Qualitative load-sinkage curves shown in Fig. 12 indicate that the point of actual failure is not as clearly defined in the fluffy model whose bearing strength is postulated to be depth

dependent as it is in the cannon ball model which is known to "yield" suddenly when the applied load overcomes the static friction and cohesion along a critical plane. Bearing strength, in this case, is defined as the normal load which can be imposed upon the surface of a soil before the system fails in shear. In the case of the fluffy model, it is not meaningful to speak of bearing strength, as such, without associating this strength with a given depth of sinkage.

- Nature and magnitude of forces resisting penetration: In addition to work done in compressing the fluffy model and expanding the cannon ball model, the major forces that resist the penetration of a pad in both models are those of interparticle friction and adhesion. It is very likely however, that the relative contribution of these forces differ in each model. It is reasonable to neglect adhesion in the cannon ball model because the particles have a large volume to surface ratio. We may easily assume that friction predominates as a resisting force by virtue of the fact that two relatively rough and unyielding surfaces are rubbing against each other along the plane of failure. While the particles in this model do undergo elastic and possibly plastic deformation, it is reasonable to assume that in the fluffy model the particles "give" (by rotating and/or translating) before plastic deformation takes place and that they are rarely in a position to rub against one another and develop frictional forces. Since the particles in this model are inherently very fine (hence susceptible to attractive forces) and a great number of them are contained within a unit area of the failure plane, adhesional forces will play a predominant role. Consequently, an important factor in predicting the bearing strength of fluffy soils is a knowledge of the number of particle bonds that are severed during failure, and the strength of each bond. The latter could depend upon the environment or, (as would be the case on the moon) upon the ambient vacuum. The number of severed bonds will depend upon the initial and final porosity of the system as well as on the depth of the "bulb" of compacted soil formed under the pad. The experimental model described in the next section was developed and tested in an attempt to verify the postulated model and clarify some of the questions discussed above.

Experimental Investigation of Fluffy Model

A crude experimental model of the fluffy soil was built so as to observe the movement of soil particles in and around the disturbed zone and determine the thickness of the "bulb" formed under the pad at various stages of penetration. This was accomplished by using a plexiglass container (4 x 4 inches square and 10 inches high) in which all four sides were scored with black horizontal lines 1/4-inch apart. The container was filled with loosely sifted alternating 1/4-inch red and gray layers of very fine fluffy powders, the interface of the layers roughly corresponding to the horizontal markings, as shown in Fig. 11a. An average porosity of 65 percent was estimated for the soil in the container on the basis of weight and volume measurements and an average "real" density of 2.5 g/cm^3 for the powders used. The gray powder is ground basalt (particle size $\leq 37\mu$) and the red powder is made up of synthetic "microballoons."

A 1-inch thick perforated cap having 1 x 1/2-inch cutouts at the middle of each side was fitted tightly on top of the container to serve as a guide for 1 x 1/2-inch rectangular wooden bars that were used as plungers. The 1-inch side of the plunger faced the inner side of the container wall as shown in Fig. 11b, c, and d. The plungers were pushed into the soil by hand at all four sides and photographs were taken at various depths of penetration. No attempt was made to measure depth versus sinkage since the primary object of the experiment was to observe the behavior of the soil during compaction or failure. The four sequential photographs of side No. 3 shown in Fig. 11 are typical of all sides in depicting the soil "profile" during the experiment.

The photographs corroborate some of the points we postulated above and clarify other points that were left in doubt. The following preliminary comments may be made on the basis of visual examination of Figs. 11b, c, and d.

- Boundaries of the disturbed zones: As postulated, the disturbed zone is limited to the area immediately under the pad. No lateral movement of soil or disturbance of the surrounding surface (as would be encountered in the cannon ball model) is observed. We also notice that the thickness of the disturbed zone increases with depth but not indefinitely as we suspected. According to this experiment (limited to four trials only), the compressed bulb under the pad does not seem to increase in thickness beyond a certain depth of penetration which is equal to

about three times the width of the pad. The settlement curve in this region is represented in Fig. 12 by line OA. At point A, the bulb appears to reach its maximum thickness which is about equal to the width of the pad and then stays constant. Contrary to our postulation, vertical compaction appears to stop beyond this point and instead, lateral compaction begins to occur. There is clear evidence in Fig. 11d that at these depths the compacted bulb acts as a wedge and pushes the tenuous material to the sides and compacts the surrounding quasi-stationary soil. This phenomenon is more clearly depicted in the diagram in Fig. 13 where we show a vertical line that joins the inflection points of the horizontal flow lines and deviates slightly away from the sheared plane down to a certain depth B. The system would probably reach its maximum bearing strength at depth B as no additional resisting forces are likely to be developed during penetration beyond this point. The increase in penetration resistance due to lateral compaction between levels A and B is qualitatively represented by curve AB on the settlement curve in Fig. 12. Assuming a semi-infinite medium of fluffy soil, the settlement curve indicates a nearly constant bearing strength beyond point B. In a layered model consisting of fluff over hardpan, "bottom" effects will cause the compacted bulb under the pad to fail in lateral shear instead of lateral compaction. Under these conditions, the settlement curve will level off and exhibit a "yield" point similar to the cannon ball model as depicted in Figs. 10 and 12.

- Behavior of soil within and outside of disturbed zone: The photographs in Fig. 11 clearly show the formation of a compacted bulb under the pad as we postulated, but they also reveal an unexpected disturbance of the soil below the compacted bulb as well as outside of it in the lateral direction, particularly after the bulb reaches its maximum thickness and begins to act as a wedge as mentioned above. We can approximately determine the density profile of the material in these exterior zones from the pattern of the "flow lines." This knowledge could be very useful in estimating the number of particle bonds that are severed during failure along the vertical "shear" plane.

- Nature of forces resisting penetration: The downward inclination of the flow lines toward the pad could be invoked as evidence to support our postulations that the material along the vertical wall fails in tension rather than in shear. The particles at the interface of the quasi-stationary medium and the downward moving bulb appear to pull one another down by realigning themselves until they break away. It is reasonable to state that adhesional rather than frictional forces predominate along this plane by virtue of the fact that at least one of the rubbing soil surfaces is "soft" and yielding, and does not offer sufficient normal resistance for frictional forces to develop. A second component of soil resistance comes into play when the vertically compacted bulb has reached its maximum thickness and begins to compact the soil laterally. We may conclude that the bearing strength of semi-infinite fluffy media (i.e., where there are no "bottom" effects) has two components, one of which is the tensile force needed to sever interparticle bonds at the interface between the disturbed and the quasi-stationary media and the other component is the force needed to compact the soil laterally. Both of these components build up gradually during sinkage down to a certain depth; then they are likely to remain constant. Beyond this depth, contrary to what we postulated, semi-infinite media could exhibit a bearing strength that is nearly independent of depth. This statement would imply that, theoretically, a pad or footing that applies a static pressure less that the terminal bearing strength of the fluff would sink into the medium down to a finite depth and then come to a stop; however, if the applied pressure is beyond the terminal bearing strength, the footing could sink in indefinitely (assuming we neglect friction). Both of these bearing strength components depend upon the initial and final porosity of the system. The former is known or measurable, the latter could be estimated on the basis of experimental models such as the one we described. Unfortunately, testing this particular, improvised, model is very laborious and the obtained data are rather crude. However, improvements can be made if necessary.

Future Work

The next step in the study of the fluffy model should consist of an attempt to translate the mode of failure defined in this report into an analytical expression relating bearing strength with relevant parameters that, so far as we can determine from this study, are initial porosity, grain size, pad geometry and interparticle bond, the latter being environment or vacuum dependent.

Regarding the mechanical properties of the cannon ball and the vesicular models, we hope to review existing bodies of knowledge in the fields of soil mechanics and ceramics bearing upon this subject, present experimental data and empirical expressions relating the strength of these materials to porosity, grain size, state of interparticle bond and other variables that have a bearing on the solid and radiative components of thermal conductivity as analyzed in Phase IIB.

The final objective of this program is to correlate the mechanical and thermal properties of candidate lunar surface materials as defined by the theoretical models developed in Phase I. A direct analytical correlation of these properties does not appear to be feasible. However, we are hopeful that we can correlate these properties indirectly in terms of material and geometrical variables that are common to both properties.

CONCLUSIONS

We would like to stress two important conclusions that emerge from our present analysis of the thermal and mechanical models of the lunar surface.

- The lunar thermal parameter γ, which can also be used as an index of material hardness when properly interpreted, is far more sensitive to changes of lunar nighttime temperatures than noon temperatures. However, the midnight temperature does not lead to a model of the lunar surface that is unique in terms of γ and depth, nevertheless, the model is instructive and may be complemented later by microwave data.

- Recently observed (Ref. 7) high-resolution lunar midnight temperature data, ranging from 70 to 150°K suggest that the surface of the moon is not as homogeneous on a Km-scale as it appears to be at much larger scales, and that localized areas widely differing in hardness from the consistency of fluff to that of porous rock appear to exist on the moon and are now amenable to earth-based detection and analysis. We recommend that new and better measurements of lunar nighttime temperatures be made as soon as possible and that theoretical and experimental investigations precede or follow these measurements. These investigations will be discussed in greater detail in subsequent reports.

REFERENCES

1. Bastin, J.A., "Lunar Hot Spots," Nature, Vol. 207, p. 1381, 1965.

2. Saari, J.M., and Shorthill, R.W., "The Surface Temperature of the Antisolar Point of the Moon," Icarus, Vol. 3, p. 161, 1964.

3. Buettner, J.K., The Moon's First Decimeter, NAS 7-100, 1962.

4. Petit, E., and Nicholson, S.B., "Lunar Radiation and Temperature," Astrophys. J., Vol. 71, p. 102, 1930.

5. Sinton, W., Physics and Astronomy of the Moon, Academic Press, 1962.

6. Murray, B.C., and Wildey, R.L., "The Surface Temperature Variations During the Lunar Nighttime," Astrophys. J., Vol. 139, p. 734, 1964.

7. Low, F., "Lunar Nighttime Temperature Measured at 20 Microns," Astrophys. J., Vol. 142, p. 806, 1965.

8. Piddington, J.H., and Minnett, H.C., "Microwave Thermal Radiation from the Moon," Australian J. Sci., Vol. A2, 1949.

9. Jaeger, J.C., "The Surface Temperature of the Moon," Australian J. of Physics, Vol. 6, No. 10, 1953.

10. Riemann, G.M.H.W., Die Partiellen Differential Gleichunger der Mathematischen Physick, Bond 1, p. 474, 1914.

11. Love, T.J., An Investigation of Radiant Heat Transfer in Absorbing, Emitting, and Scattering Media, ARL 63-3, 1963.

12. Wesselinck, A.J., "Heat Conductivity and the Nature of the Lunar Surface," Material Bull. Astron. Inst. of Netherlands, Vol. 10, p. 351, 1948.

13. Laubitz, M.J., "Thermal Conductivity of Powders," Can. J. Phys., Vol. 37, p. 798, 1959.

14. Schotte, W., "Thermal Conductivity of Packed Beds," A.I.Ch.E. Jour., Vol. 6, p. 63, 1960.

15. Clark, S., "Absorption Spectra of Some Silicates in the Visible and Near Infrared," American Minerologist, Vol. 142, p. 732, 1957.

16. Gehrels, T., "A Model of the Lunar Surface," Icarus, Vol. 3, p. 491

17. Hamaker, H.C., Radiation and Heat Conduction in Light Scattering Material, Philips Res. Rep., Vol. 2, p. 55, 1947.

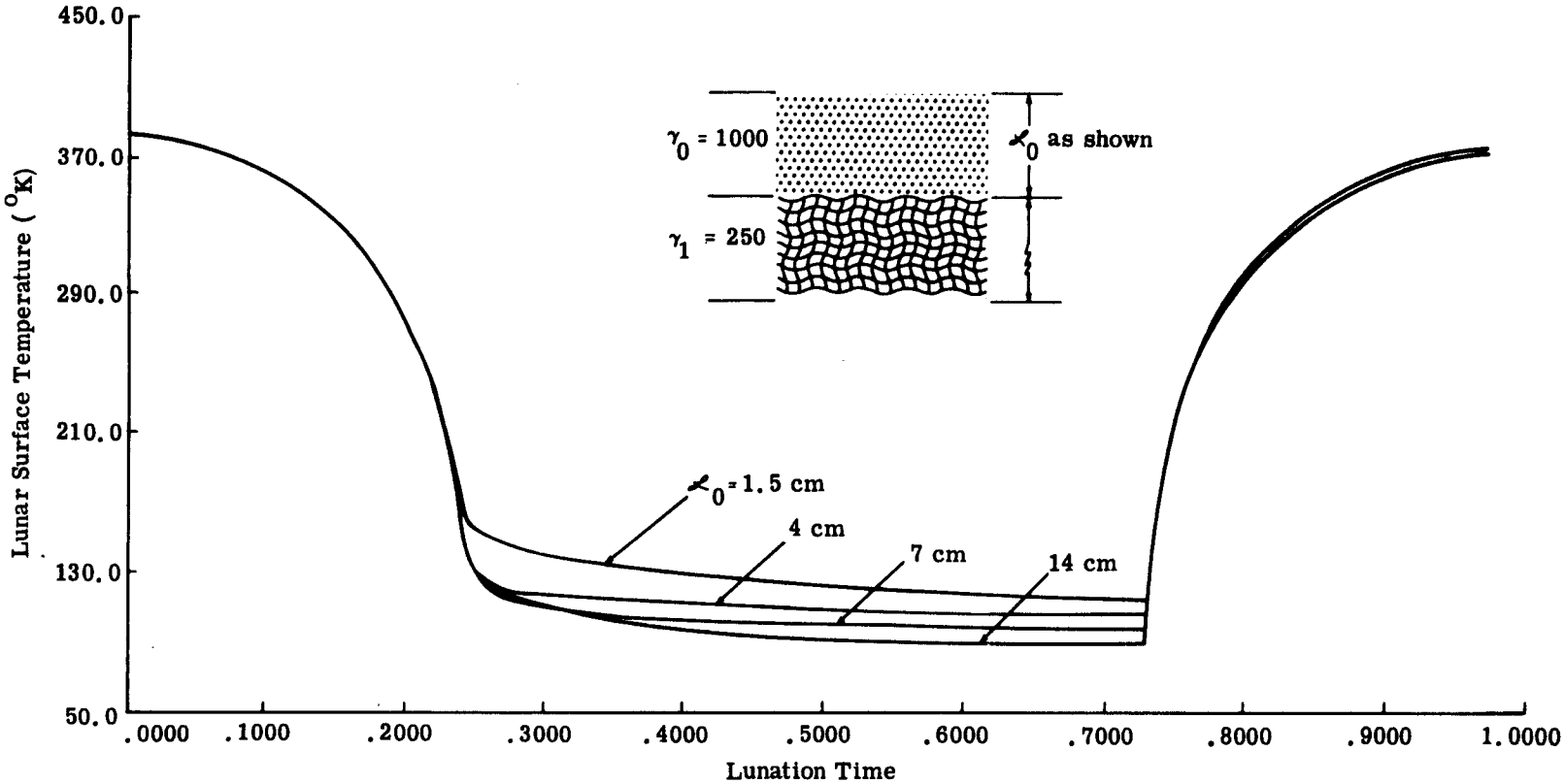

Fig. 1 Lunation Temperatures of Moon for Two-Layer Model

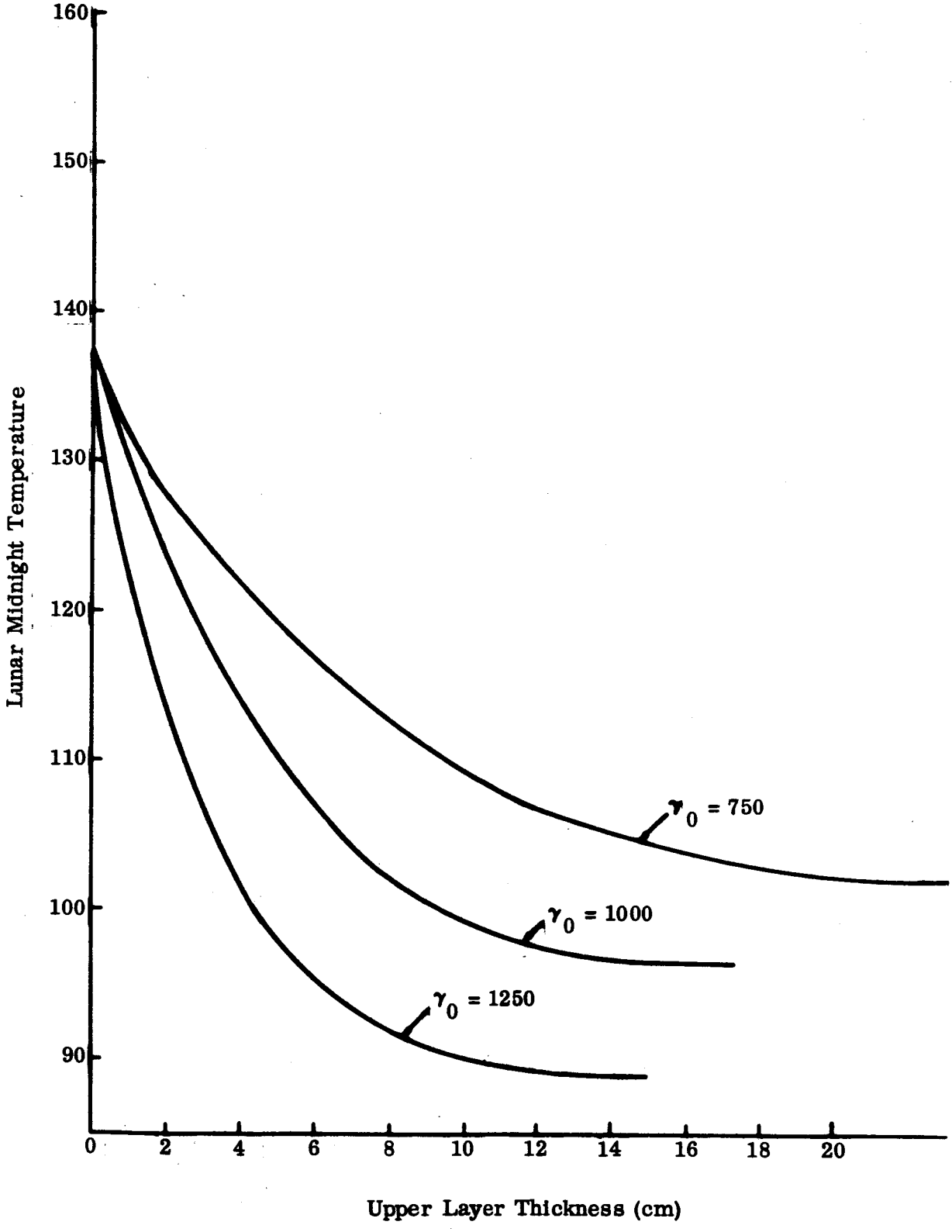

Fig. 2 Lunar Midnight Temperatures vs Upper Layer Thickness for Lower Layer $\gamma_1 = 250$ and Upper Layer γ_0 as Shown

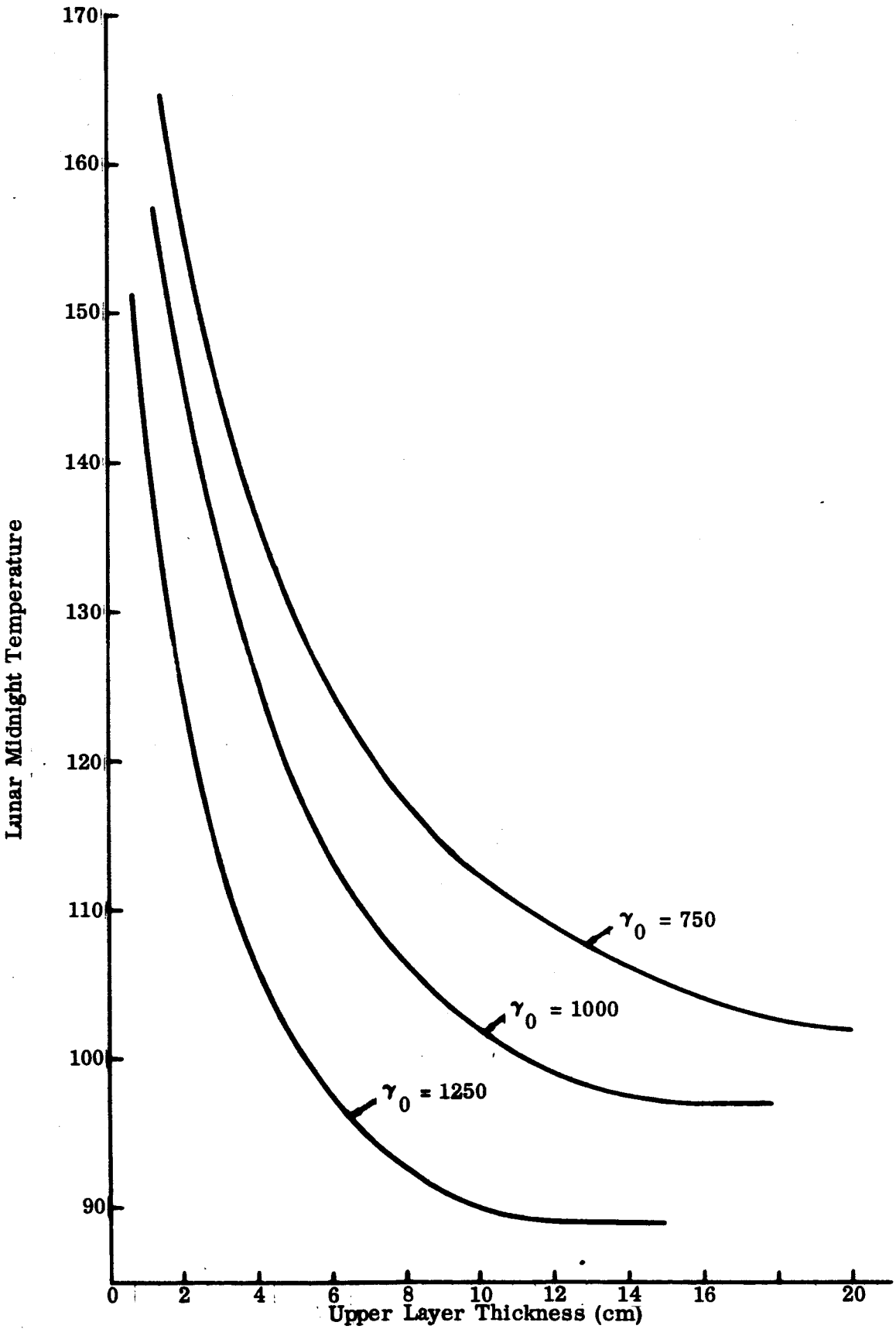

Fig. 3 Lunar Midnight Temperatures vs Upper Layer Thickness for Lower Layer $\gamma_1 = 20$ and Upper Layer γ_0 as Shown

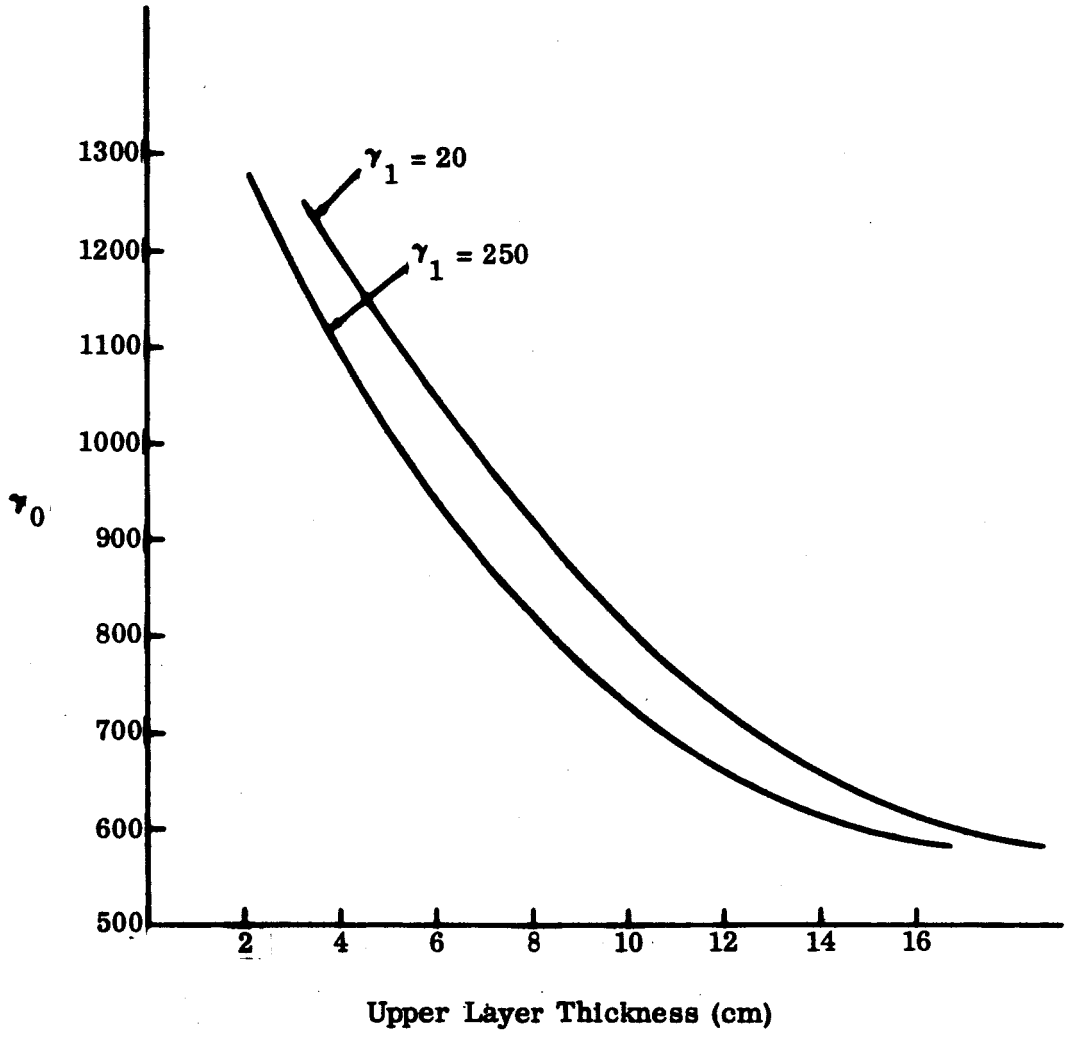

Fig. 4 γ_0 vs Thickness of Upper Layer for Midnight Temperature of 110°K Lower Layer γ_1 as Shown

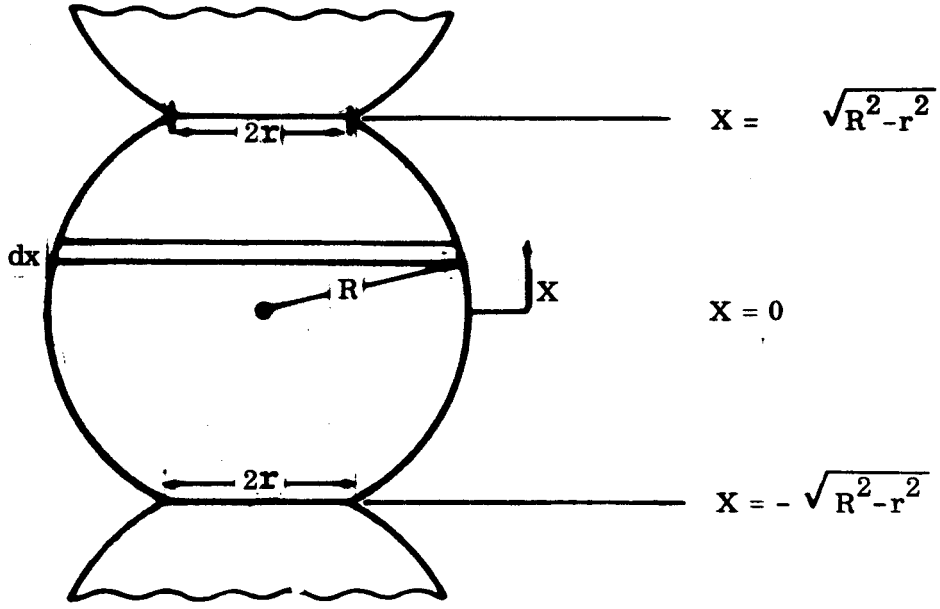

Fig. 5 Particulate Model of Solid Conduction Component

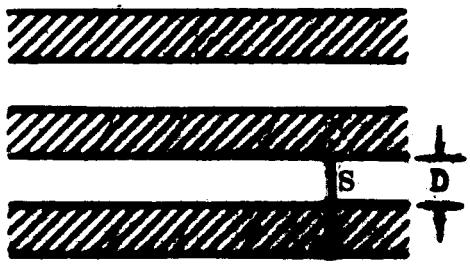

Fig. 6 Particulate Model of Radiative Conduction Component

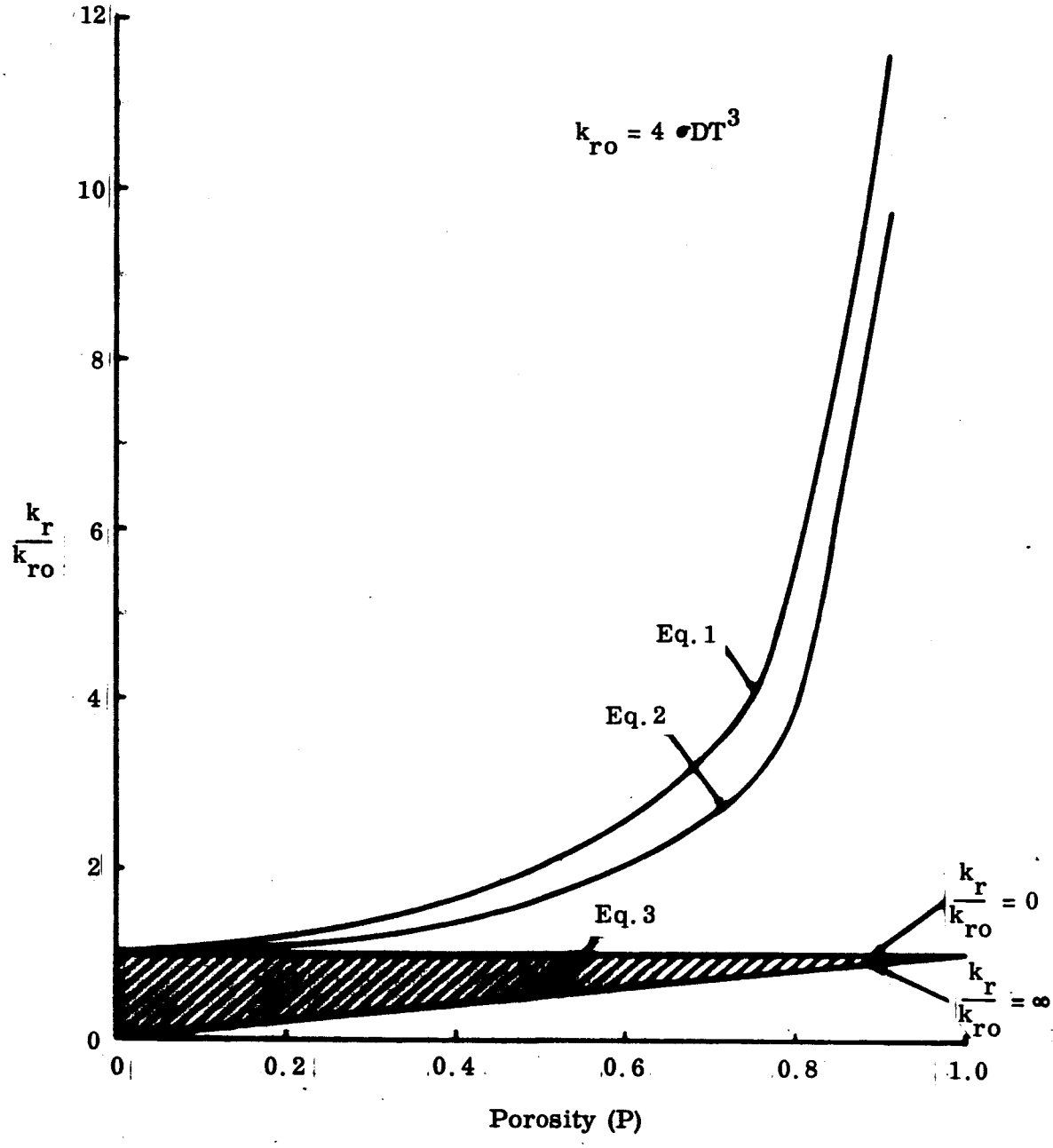

Fig. 7 Radiative Conductivity versus Porosity

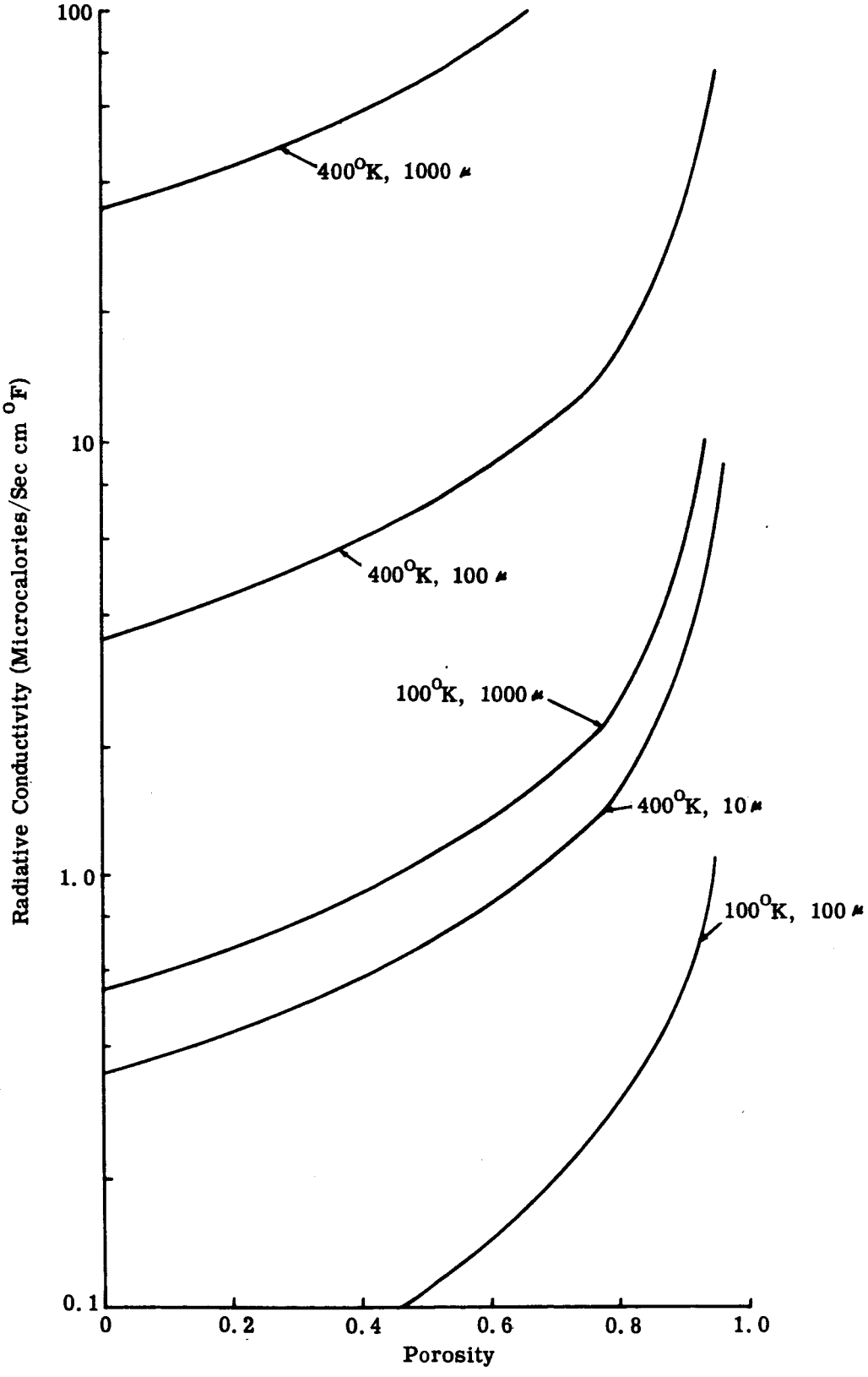

Fig. 8 Radiative Conductivity versus Porosity for Different Particle Sizes and Temperatures

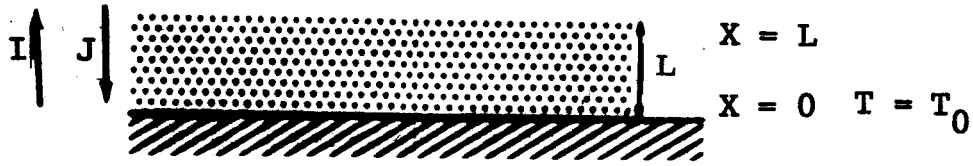

Fig. 9 Suspended Particle Model of Radiative Conduction Component

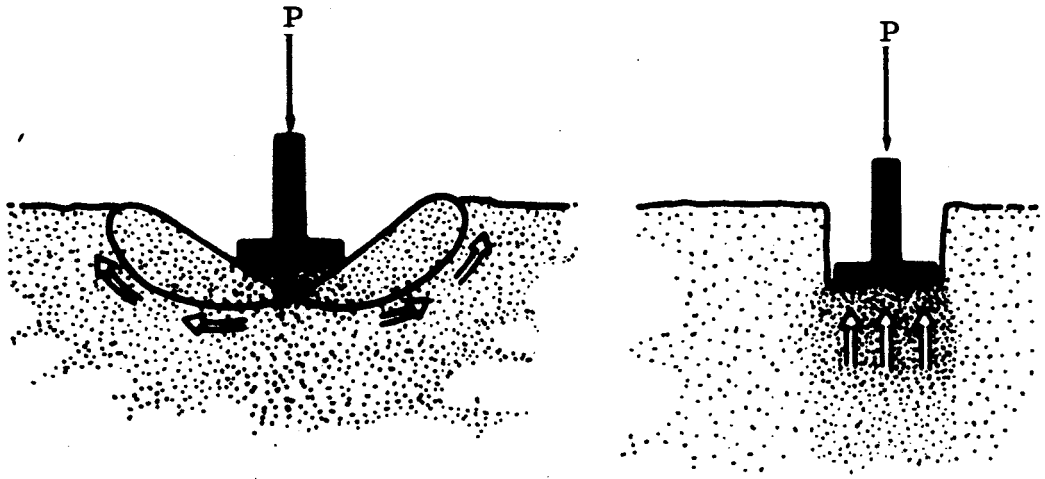

(a) "Cannon Ball" Model
Shear Failure

(b) "Fluffy" Model
Compressive Failure

Fig. 10 Modes of Failure in Particulate Media

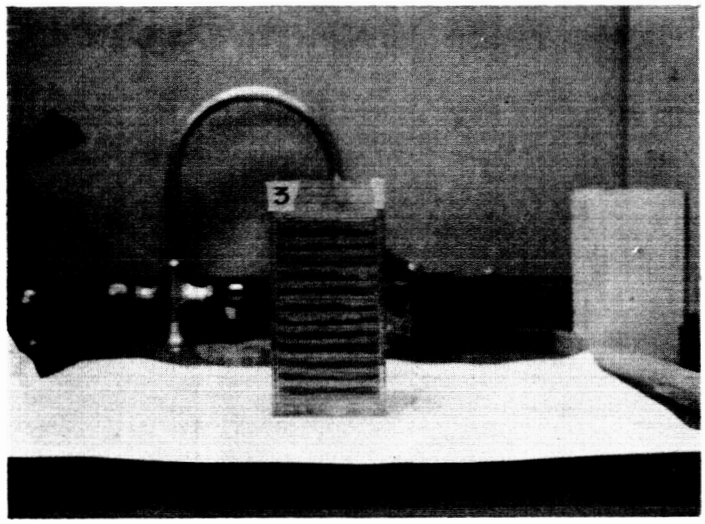

a) Undisturbed Soil

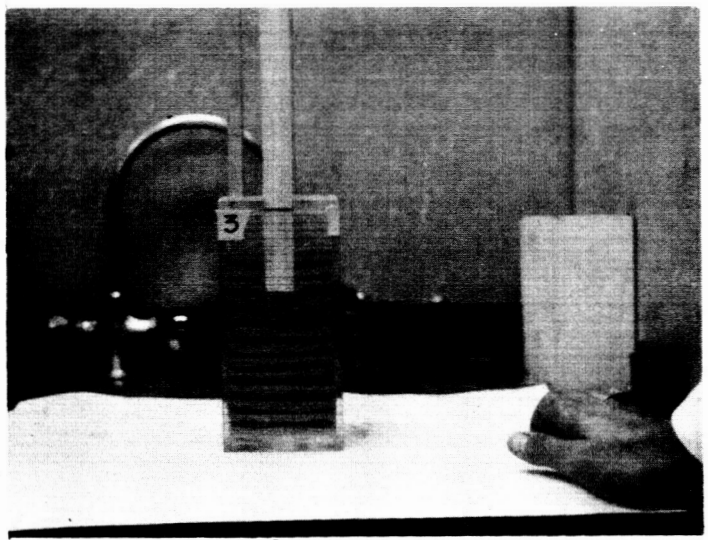

b) Penetration = $1\frac{1}{2}$" , Depth of Compressed Bulb $\approx \frac{3}{4}$"

Fig. 11 Failure Patterns on Fluffy Model

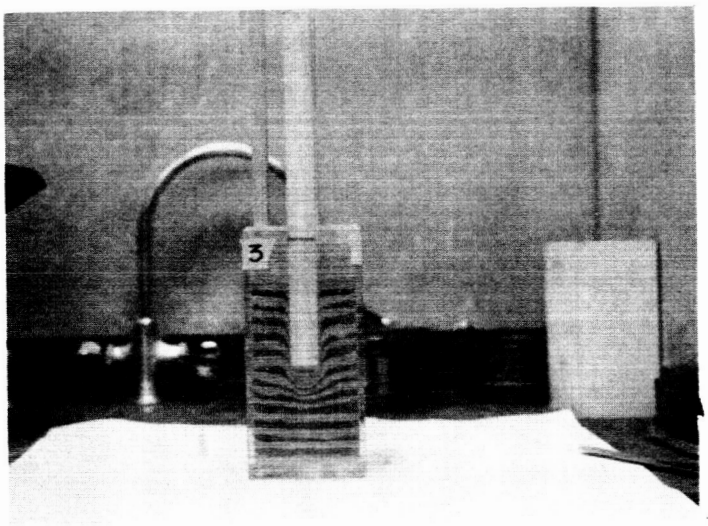

c) Penetration = 3", Depth of Compressed Bulb ≈ 1"

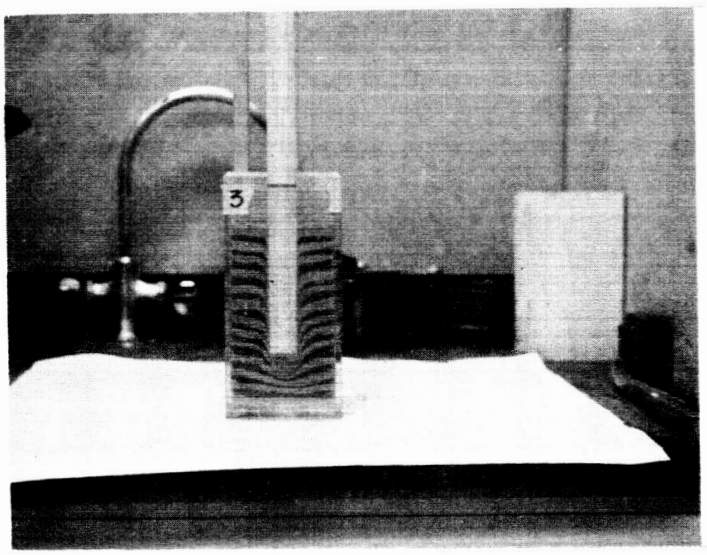

d) Penetration = $4\frac{1}{2}$" , Depth of Compressed Bulb ≈ 1"

Fig. 11(Cont.) Failure Patterns on Fluffy Model

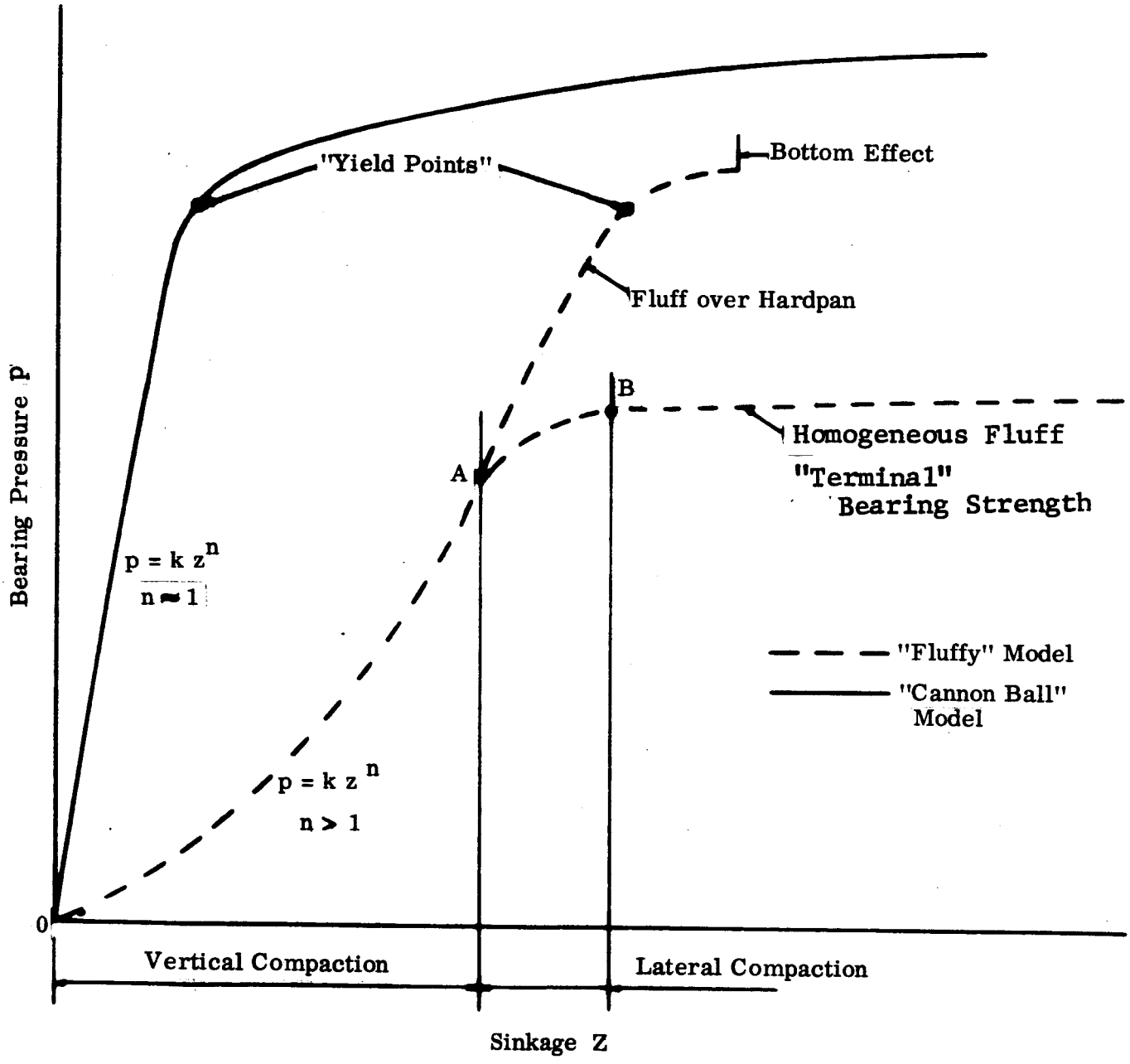

Fig. 12 Settlement Curves in Particulate Media

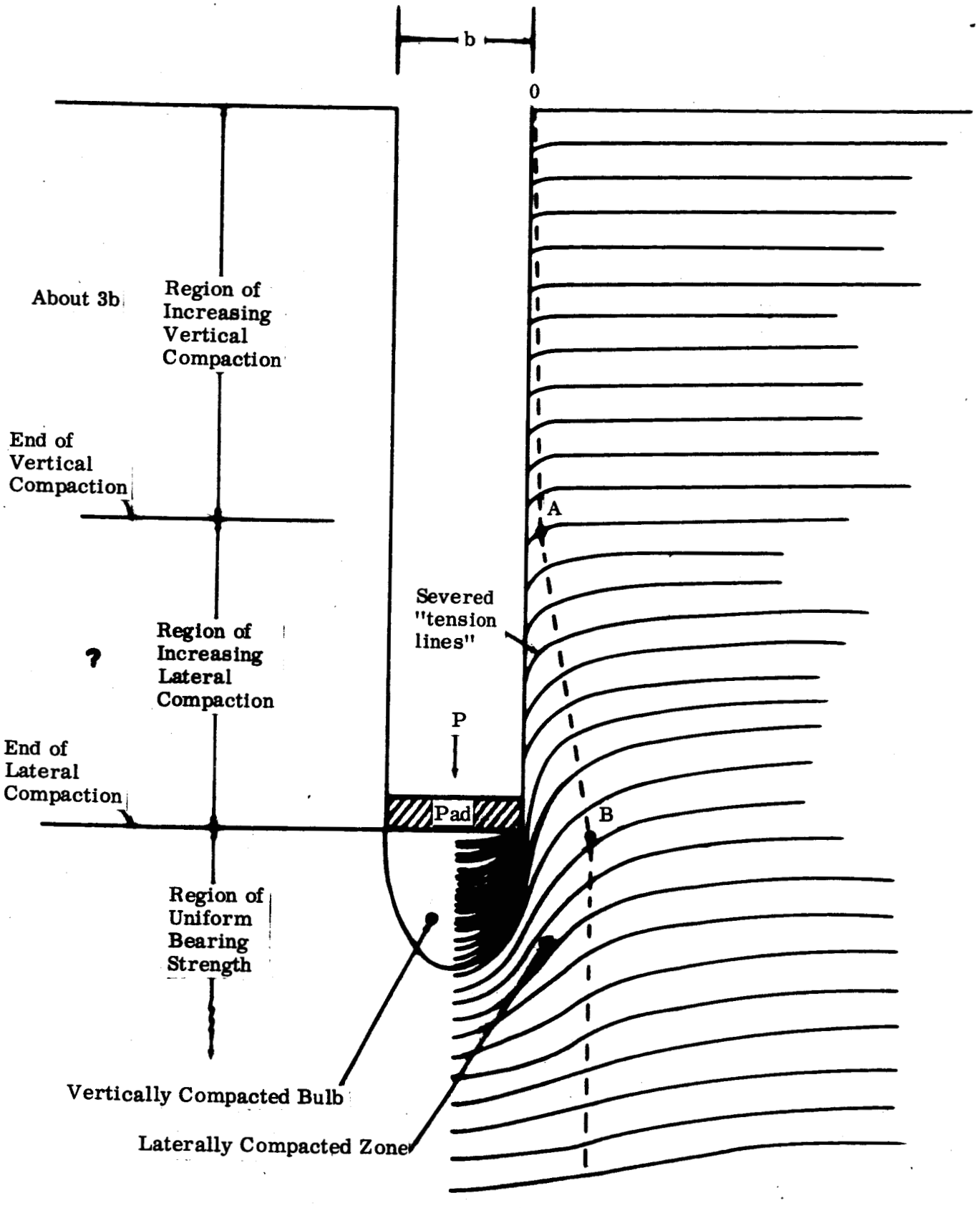

Fig. 13 Postulated Failure Mode in Semi-infinite Fluffy Medium


Grumman
GRUMMAN AIRCRAFT E
BETHPA
NEW YOR